Check for updates

Radiative pumping in a strongly coupled microcavity filled with a neat molecular film showing excimer emission†

Yoichi Sasaki, [ID] ⋆[ab] Kyriacos Georgiou, [ID] ‡[b] Shuangqing Wang,[b] David G. Bossanyi, [ID] [b] Rahul Jayaprakash,[b] Nobuhiro Yanai, [ID] [a] Nobuo Kimizuka, [ID] [a] David G. Lidzey,[b] Andrew J. Musser [ID] [c] and Jenny Clark [ID] ⋆[b]

Strong light-matter interactions have attracted much attention as a means to control the physical/chemical properties of organic semiconducting materials with light-matter hybrids called polaritons. To unveil the processes under strong coupling, studies on the dynamics of polaritons are of particular importance. While highly condensed molecular materials with large dipole density are ideal to achieve strong coupling, the emission properties of such films often become a mixture of monomeric and excimeric components, making the role of excimers unclear. Here, we use amorphous neat films of a new bis(phenylethynyl anthracene) derivative showing only excimer emission and investigate the excited-state dynamics of a series of strongly coupled microcavities, with each cavity being characterised by a different exciton–photon detuning. A time-resolved photoluminescence study shows that the excimer radiatively pumps the lower polariton in the relaxation process and the decay profile reflects the density of states. The delayed emission derived from triplet–triplet annihilation is not sensitive to the cavity environment, possibly due to the rapid excimer formation. Our results highlight the importance of controlling intermolecular interactions towards rational design of organic exciton–polariton devices, whose performance depends on efficient polariton relaxation pathways.

Introduction

Exciton–polaritons are quasi-particles generated through strong interaction between excitons and photons. When the energy exchange between an excitonic transition and a confined optical field is much faster than the rate of energy dissipation, the strong interaction results in the formation of two new hybridised states (Fig. 1a). These states are called upper polariton (UP) and lower polariton (LP), and the newly formed energy levels are separated in energy by the so-called Rabi splitting. Being composite bosons, in conjunction with the fact that they possess reduced effective mass inherited by the

[a] *Department of Chemistry and Biochemistry, Graduate School of Engineering, Center for Molecular Systems (CMS), Kyushu University, 744 Moto-oka, Nishi-ku, Fukuoka 819-0395, Japan. E-mail: sasaki.yoichi.772@m.kyushu-u.ac.jp*

[b] *Department of Physics and Astronomy, The University of Sheffield, S3 7RH, Sheffield, UK. E-mail: jenny.clark@sheffield.ac.uk*

[c] *Department of Chemistry and Chemical Biology, Cornell University, Ithaca, New York 14853, USA*

† Electronic supplementary information (ESI) available. See DOI: https://doi.org/10.1039/d4cp00255e

‡ Present address: Department of Physics, Laboratory of Ultrafast Science, University of Cyprus, Nicosia 1678, Cyprus.

photons involved, exciton–polaritons can undergo Bose–Einstein condensation and superfluidity at relatively higher temperatures as compared to traditional atomic condensates.[1–3]

Organic semiconductors, in particular, have long been good material candidates for exciton–polariton research since the transition dipole moment leads to a large Rabi splitting ($\hbar\Omega_{Rabi}$, 0.1–1 eV) and the strong binding energy of Frenkel-excitons stabilizes the exciton–polaritons to be realised at room temperature.[4–8] Since the formation of polaritons can enable manipulation of potential energy surfaces of materials, photophysical/chemical processes such as photoisomerization,[9,10] reverse intersystem crossing,[11–14] energy transfer,[15–20] singlet fission,[21–23] and triplet–triplet annihilation[24–26] have been investigated under strong coupling.

Understanding polariton dynamics has been an important challenge in recent studies. So far, two polariton populating processes are proposed based on experiments and theoretical studies: vibrationally assisted scattering (VAS) and radiative pumping (Fig. 1b). VAS is a rapid relaxation process involving a hot exciton populating the LP state by the emission of a low-energy vibrational quantum through intramolecular exciton–phonon coupling.[27–29] The radiative pumping mechanism is explained by incoherent emission from the intracavity dark

This journal is © the Owner Societies 2024

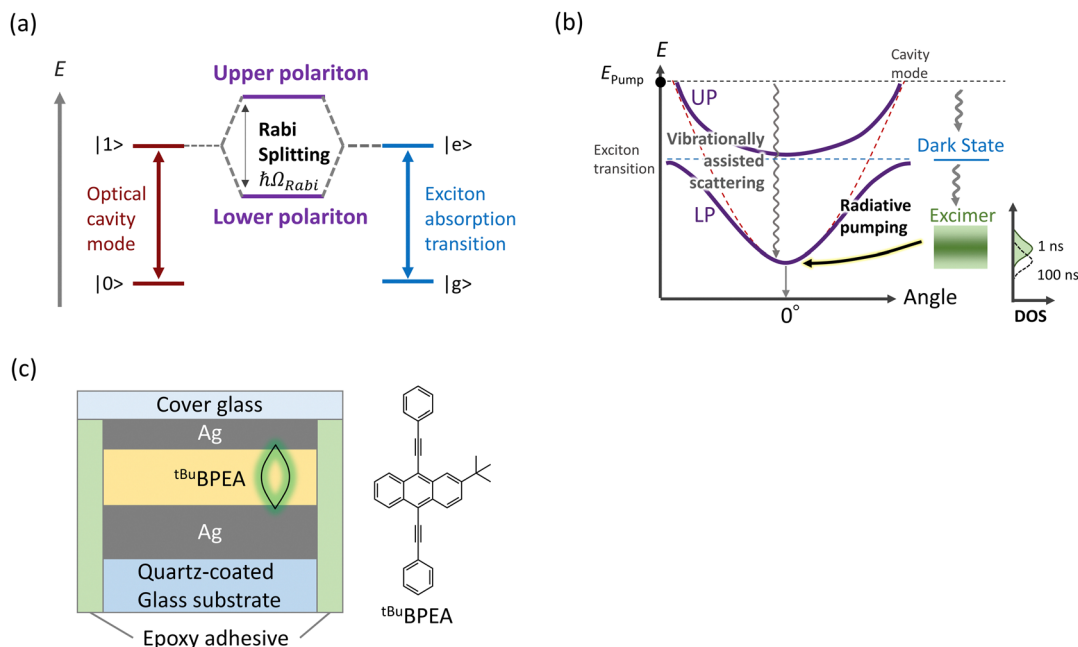*Phys. Chem. Chem. Phys.*, 2024, **26**, 14745–14753 | **14745**

Fig. 1 (a) Formation of hybrid polaritonic states as a result of strong light-matter interactions. (b) Angular dispersion of lower polariton and upper polariton states (purple), cavity mode (red), and exciton transition (blue) along with the proposed relaxation mechanism of the organic exciton–polaritons. The ^{tBu}BPEA film shows the change in density of state (DOS) over time in the excimer state. (c) Schematic of the cavity structure studied and the chemical structure of ^{tBu}BPEA.

state that populates the LP state, resulting in similar decay profiles to the active layer.[30–34] Interestingly, in the presence of electronic coupling between an excited singlet state and a triplet pair state, the delayed PL, originally from triplet–triplet annihilation, has been found to be altered under strong coupling.[24] Further studies from nanosecond to microsecond timescales are necessary to unveil the population dynamics of exciton–polaritons.

To simplify the photophysical processes of the microcavity active material, it is important to control the morphology of the semiconductor. Typical Fabry–Pérot cavities consisting of two parallel mirrors require a high loading of dye, which can lead to inhomogeneous optical responses due to partial crystallization or segregation from the host. Furthermore, when the photoluminescence (PL) of a film shows both monomeric and excimeric emission, understanding the origin of the PL dynamics under strong coupling becomes complex. For these reasons, amorphous molecular glass with a single emission component could be an ideal candidate for exciton–polariton studies, given its isotropic feature and processability.

Here, we design the new molecule 2-(*tert*-butyl)-9,10-bis(phenylethynyl)anthracene (^{tBu}BPEA) that forms molecular glass in the solid state, and the polariton PL dynamics of strongly coupled microcavities with the molecule are investigated (Fig. 1c). Substitution with a *tert*-butyl group at the 2nd position of BPEA makes the structure non-symmetric, resulting in the formation of a stable amorphous neat film at room temperature. The PL of the film is dominated by excimer emission, which allows us to study the contribution of the excimer state to the polariton dynamics. When the film is

placed between silver mirrors, the high dipole density enables strong coupling of the cavity mode and excitonic transition. The LP branch substantially overlaps in energy with the excimer emission, resulting in a strong LP emission and an excimer emission. Since the excimer is formed through intermolecular interactions in the excited state, this state does not contribute to the transition dipole moment coupled with the optical cavity mode after relaxation yet acts as an uncoupled exciton reservoir that radiatively populates the LP state. The broad emission spectra allow us to investigate the wavelength-dependent PL dynamics of the cavity samples. Based on the transient absorption and time-resolved PL of the neat film, we discuss the possible decay dynamics of the strongly coupled microcavities.

Experimental

Instrumentation

^{1}H-NMR (400 MHz) spectra were measured on a JEOL JNM-ECZ400S using TMS as the internal standard. Elemental analysis was conducted at the Elemental Analysis Center, Kyushu University. UV-Vis absorption spectra were recorded on a JASCO V-670 spectrophotometer and a Horiba Fluoromax 4 fluorometer utilising a Xenon lamp. PL spectra were measured using a JASCO FP-8700 NIR spectrofluorometer.

Materials and methods

All reagents and solvents were used as received without further purification otherwise noted. 2-*tert*-Butylanthracene and phenylacetylene were purchased from TCI, bromine was purchased

14746 | *Phys. Chem. Chem. Phys.*, 2024, **26**, 14745–14753

This journal is © the Owner Societies 2024

from Wako. CuI and Pd(dppf)$_2$Cl$_2$ were purchased from Sigma Aldrich.

Synthetic procedures

Synthesis of 2-(*tert*-butyl)-9,10-dibromoanthracene (*tBu*DBA). 1.64 g (7 mmol) of 2-*tert*-butylanthracene was dissolved into 20 mL of CH$_2$Cl$_2$ under N$_2$ condition and cooled to 0 °C with an ice bath. 0.75 mL (*ca.* 14 mmol) of bromine was added and the solution was stirred without the bath to gradually return to room temperature. The solution was stirred for 4.5 hours and 5 mL of 10 wt% NaHSO$_4$ aqueous solution was added. The solution was washed with a mixed solution of CH$_2$Cl$_2$ and H$_2$O (CH$_2$Cl$_2$:H$_2$O = 1:1). After drying with Na$_2$SO$_4$, the solution was evaporated, and the solid was washed with a tiny amount of MeOH and filtrated. The compound was used without further purification. (2.2 g, 80%) ^{1}H-NMR (400 MHz, chloroform-*d*) δ (ppm) 8.61–8.55 (m, 2H), 8.52 (d, *J* = 5.0 Hz, 1H), 8.49 (d, *J* = 1.6 Hz, 1H), 7.73 (dd, *J*$_1$ = 4.5 Hz, *J*$_2$ = 1.8 Hz 1H), 7.63–7.60 (m, 2H), 1.49 (s, 9H).

Synthesis of 2-(*tert*-butyl)-9,10-bis(phenylethynyl)anthracene (*tBu*BPEA). 784.9 mg (*ca.* 2 mmol) of *tBu*DPA and 30.7 mg (0.16 mmol) of CuI were dissolved into a mixed solution of THF and diisopropylamine (THF:diisopropylamine = 25 mL: 25 mL) under N$_2$ atmosphere. 0.48 mL (4.4 mmol) of phenyl acetylene and 98.1 mg (0.12 mmol) of Pd(dppf)Cl$_2$ were added and refluxed for 2 hours at 100 °C with microwave radiation (Biotage Initiator 2.5). The solution was mixed with 150 mL of deionized water and filtrated. The residue was separated with a mixed solution of CHCl$_3$ and water (CHCl$_3$:water = 1:1) three times and the organic layer was dried with Na$_2$SO$_4$. After concentration, the compound was purified by a silica gel column chromatography with CHCl$_3$ and hexane (CHCl$_3$:hexane =1:9 and 1:4). (300 mg, 35%) ^{1}H-NMR (400 MHz, chloroform-*d*): δ (ppm) 8.7–8.63 (m, 4H), 7.79–7.75 (m, 5H), 7.65–7.60 (m, 2H), 7.49–7.40 (m, 6H), 1.53 (s, 9H), Elemental analysis: calculated for C$_{34}$H$_{26}$:C 93.97 H 6.07 N 0.00, found C 93.78 H 6.01 N 0.00.

Transfer matrix simulation of microcavity with *tBu*BPEA

Microcavities were designed with transfer matrix simulation. The absorption of a neat *tBu*BPEA film with 75 nm thickness was measured and fitted with two Lorenz functions to obtain the complex dielectric constant based on Kramers–Kronig relationship. We estimated the thickness range corresponding to detuning from positive to negative (Fig. S2, ESI†). The full width at half maximum of the cavity mode was estimated to be 55 meV by eliminating the contribution of exciton peaks (Fig. S3, ESI†).

Microcavity fabrication

Ag mirrors were evaporated using an Ångstrom Engineering thermal evaporator installed into a glovebox ([O$_2$] < 0.1 ppm). The sample chamber was held at a base pressure of 2 × 10^{-6} mbar and the deposition rate was kept between 0.5 and 1 Å s^{-1}. The bottom mirror had a thickness of 200 nm while the top mirror was semi-transparent having a thickness of 55 nm. The organic layers were spin-coated on quartz coated glass

substrates or on top of the 200 nm bottom Ag mirror (substrates 20 mm × 15 mm, Ossila Ltd) from a THF solution of *tBu*BPEA ([*tBu*BPEA] = 15 mg mL^{-1}). The thickness of the cavity's active layer was controlled by changing the velocity of rotation in the range of 2000–5000 rpm to create λ/2-mode cavities in resonance with the *tBu*BPEA excitonic transition. In all cases, uniform films were created. Cavities with intended *tBu*BPEA thicknesses between 90 nm and 125 nm with 5 nm step (C90–C125) and a 100 nm bare film sample (B100) were fabricated. We found thickness differences depending on the position of the probe light in the reflectivity measurements, which is possibly due to the curved surface in the semiconductor layer formed during the spin coating. Samples C90, C100, C110, C120 and B100 were sealed with a glass plate and Araldite, while in an N$_2$ environment, to prevent quenching of triplet by oxygen in time-resolved PL measurements (Fig. 1c and Fig. S4, ESI†). All samples were prepared in the glovebox on the same day to keep the encapsulation conditions similar.

Angle-resolved white light reflectivity and PL

Angle-resolved white light reflectivity measurements were performed using a goniometer setup consisting of two motorised rotation arms. A fibre-coupled Halogen-Deuterium white light source (DH-2000-BAL, Ocean Optics) was focused on the sample's surface using a series of lenses attached to the first arm. Reflected light was first collimated and then focused into an optical fibre through a series of lenses mounted on the second arm and finally sent into an Andor Shamrock SR-303i-A CCD spectrometer. For angular dependent PL measurements, samples were excited close to normal incidence using a 405 nm CW laser diode. The same motorised arm used to collect light in reflectivity measurements was also used to collect PL emission from the cavity. PL intensity was assumed to follow the ideal Lambertian profile,

$$I(\theta) = I_0 \cos\theta \qquad (1)$$

Polariton population P_{pol} was calculated by dividing I_0 by the square of the photonic component of the Hopfield coefficient $|\alpha_\gamma|^2$.[15]

$$P_{pol} \propto \frac{I(\theta)}{\cos\theta |\alpha_\gamma|^2} \qquad (2)$$

Three-level coupled oscillator model[35,36]

The following three level coupled oscillator model was used to describe strong coupling in the microcavities,

$$\begin{pmatrix} E_\gamma(\theta) & g_1 & g_2 \\ g_1 & E_1 & 0 \\ g_2 & 0 & E_2 \end{pmatrix} \begin{pmatrix} \alpha_\gamma \\ \alpha_1 \\ \alpha_2 \end{pmatrix} = E_p \begin{pmatrix} \alpha_\gamma \\ \alpha_1 \\ \alpha_2 \end{pmatrix} \qquad (3)$$

where $E_\gamma(\theta)$, E_1 and E_2 denote the energies of the cavity mode and the excitonic transitions as described by two Lorentz curves, with g_1 and g_2 being the values of the interaction potential. The eigenvectors α_γ, α_1 and α_2 represent the Hopfield coefficients of the strongly coupled system. The angle-dependent energy of the

This journal is © the Owner Societies 2024

Phys. Chem. Chem. Phys., 2024, **26**, 14745–14753 | **14747**

cavity mode was calculated using the following expression

$$E_\gamma(\theta) = E_0 + \frac{\hbar^2}{2m_{cav}e}\left(\frac{2\pi}{\lambda_0}n_{cav}\sin\theta\right)^2 \quad (4)$$

$$m_{cav} = \frac{\pi\hbar n_{cav}}{cL}, \quad n_{cav} = \frac{\pi\hbar c}{E_0 eL} \quad (5)$$

where m_{cav} and n_{cav} are the effective mass and refractive index respectively. Diagonalization of the Hamiltonian gives rise to three unique solutions describing the three polariton branches formed, with the energy of the LPB at $k_{//} = 0$ and the coupling constants being shown in Table S1 in the ESI.†

Density functional theory (DFT) calculation

Density functional theory (DFT) and time-dependent DFT (TD-DFT) calculations were conducted with the WB97XD exchange–correlation functional as implemented in the Gaussian 09 software.[37] As basis sets, 6-311G(d,p) and 6-311G(d,p)++ were used, respectively. Frequency analyses were also conducted to ensure that the converged structures reached the potential energy minimums.

Time-resolved PL

The time-resolved photoluminescence spectra were recorded *via* a time-gated intensified charge-coupled device (iCCD; iStar DH334T-18U-73, Andor), coupled to a Shamrock 303i spectrograph. Excitation pulses at 400 nm were generated by frequency doubling of the 800 nm laser fundamental of Ti:Sapphire laser (Solstice, Spectra-Physics) using a β-barium borate crystal (BBO-604H, θ = 29.2°, 1 mm thickness, EKSMA Optics), with subsequent filtering of the residual 800 nm using an absorptive filter (Schott BG39 FBG-3925, 3 mm thickness, UQG Optics). The excitation was performed at normal incidence and it was collinear to the detection path. Residual excitation pulses after the sample were removed with an absorptive long-pass filter (Schott GG435 FGG-43525, 3 mm thickness, UQG Optics). Further details regarding the TRPL data processing have been reported previously.[38]

Picosecond transient absorption (TA) spectroscopy

Picosecond transient absorption spectroscopy was undertaken with a commercial spectrometer (Helios, Ultrafast Systems) outfitted with a Ti:Sapphire seed laser (MaiTai, Spectra-Physics) providing 800 nm pulses (84 MHz, 25 fs nominal FWHM) and a Ti:Sapphire regenerative amplifier (Spitfire Ace
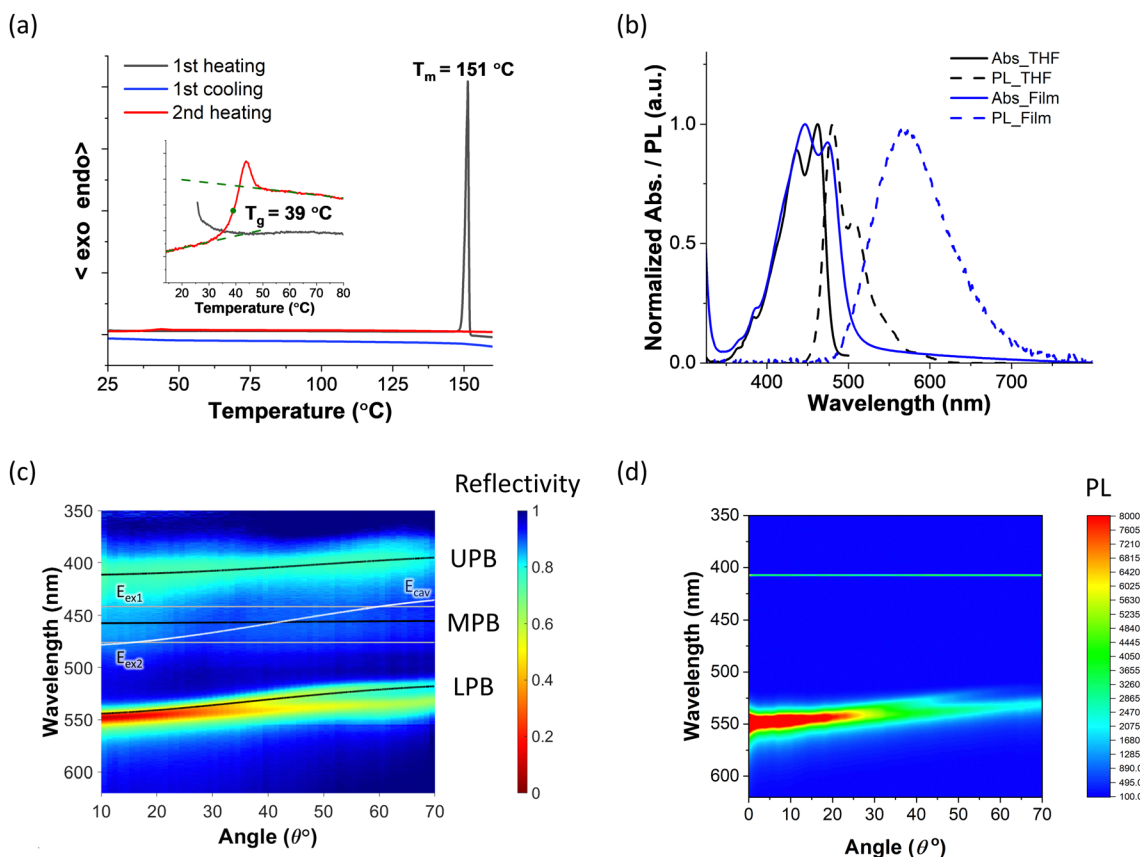

Fig. 2 (a) Differential scanning calorimetry curve of ^{tBu}BPEA. Inset shows the enlarged data from 15 °C to 80 °C. (scan rate: 2 °C min^{-1}) (b) Absorbance and PL spectra of ^{tBu}BPEA in tetrahydrofuran (THF) and in the neat film. Note that the reflection was not taken into consideration in the neat film. Angle-dependent (c) reflectivity along with a fit using a coupled–oscillator model and (d) PL (λ_{ex} = 400 nm) of C115 cavity. UP, MP, LP branches (UPB, MPB, LPB) are shown in black.

14748 | *Phys. Chem. Chem. Phys.*, 2024, **26**, 14745–14753

This journal is © the Owner Societies 2024

PA-40, Spectra-Physics) amplifying 800 nm pulses (10 kHz, 12 W average power, 40 fs nominal FWHM). 400 nm pump pulses were generated by seeding a part of the 800 nm beam into a frequency doubler utilizing β-barium borate crystals (TimePlate, Photop Technologies). An optical chopper was used to modulate the pump frequency to 5 kHz. A variable neutral density filter was used to tune the average pump power incident on the sample to 1 mW; this was measured slightly before the sample position (off-focus) with a photodiode power sensor (S120VC, Thorlabs) and meter console (PM100D, Thorlabs). Supercontinuum probes were generated with a part of the 800 nm pulse focused on a continuously translating CaF$_2$ crystal. Pump–probe delay was controlled with a motorized delay stage. The signal was dispersed with a grating and detected with a CMOS sensor. The pump and probe polarizations were set to the magic angle. The room temperature was controlled at 19 °C. The TA data were processed by background subtraction and chirp correction.

Results and discussion

Thermal properties

$^{t\mathrm{Bu}}$BPEA exhibit a melting signal only in the first heating process (T_{m} = 151 °C) and a crystallization peak was not observed (Fig. 2a), indicating the formation of amorphous phase as seen in 2,9,10-phenylanthracene (T_{m} = 209 °C).[39] This assignment is consistent with the powder X-ray diffraction (PXRD) in which crystalline peaks disappeared after annealing at 170 °C (Fig. S5, ESI†). The glass transition temperature (T_{g}) was estimated to be 39 °C. Therefore, $^{t\mathrm{Bu}}$BPEA can form a stable molecular glass at room temperature, which is ideal for measurements of optical response under strong coupling.

Absorption and PL spectra

The spin-coated films of $^{t\mathrm{Bu}}$BPEA showed different oscillator strengths among vibronic peaks from the THF solution (Fig. 2b). The 0–1 transition appears to have a stronger intensity than the 0–0 transition, which indicates H-type intermolecular interactions in the ground state.[40,41] The broad and red shifted PL of the film was assigned to excimer emission reported in BPEA dimers or aggregates.[41,42] Since dense aggregation facilitates excimer formation in the excited state, only excimer emission was observed in our films.

Angle-dependent reflectivity and PL spectra

Hybridization of a cavity mode with the two excitonic transitions of $^{t\mathrm{Bu}}$BPEA results in the formation of three new polaritonic states (Fig. 2c and Fig. S6–S9, ESI†). The formed polariton
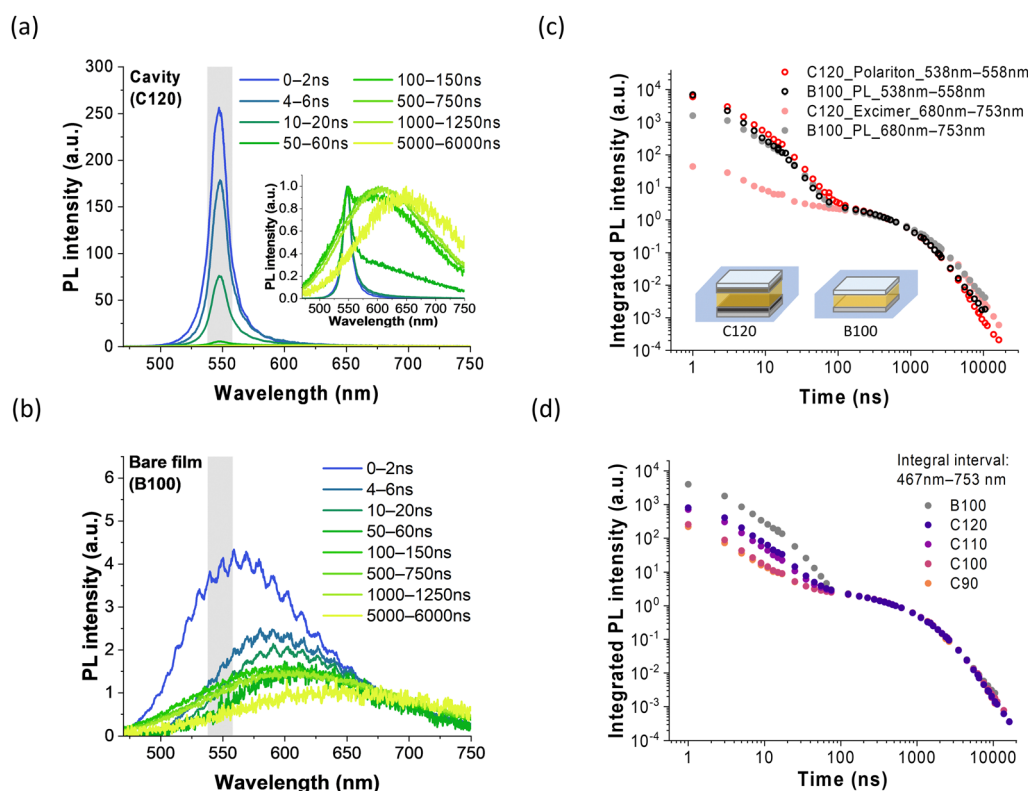

Fig. 3 Time-dependent PL spectra for (a) C120 cavity and (b) a bare film (B100, λ_{ex} = 400 nm, P_{ex} = 1.3 mJ cm^{-2}). In both parts (a) and (b), the spectra are normalised at 680 nm where all cavity samples exhibit similar PL decay profiles. The spectra in the inset of part (a) have been normalized at the wavelength with the maximum PL intensity. (c) The decay profiles of the integrated PL intensity for the cavity C120 under the integration range corresponding to the LP (red, 538–558 nm) and part of the excimer emission (680–753 nm). The decay profiles for the bare film B100 (grey) with the same integration ranges are also plotted for reference. (d) The decay profiles of the integrated PL for B100, C90, C100, C110, and C120. The integral interval covers the entire detected wavelength range from 467 nm to 753 nm.

This journal is © the Owner Societies 2024

Phys. Chem. Chem. Phys., 2024, **26**, 14745–14753 | **14749**

states exhibit an anti-crossing behaviour over the angular range probed, which is a key manifestation of the strong coupling regime.[36] The strength of the interaction, or the rate of energy exchange between excitons and photons, is estimated by the Rabi splitting which we define as the minimum energy splitting between consecutive polariton states (Fig. 1a). We have used a classical three level coupled-oscillator model to fit the reflectivity data of the cavities.[4,43] In Fig. 2c and Fig. S6–S9 in the ESI,† the experimental angular dispersion data were overlaid with the eigenvalues calculated with our coupled oscillator model (black solid lines), and these simulations and experiments showed excellent agreement. The Rabi splitting in the series of cavities we studied was estimated to be around 0.5 eV, which is much larger than the full width at half maximum of the estimated optical mode and excitonic transitions (Fig. S3 and Table S1, ESI†), placing our cavities in the strong coupling regime.[44] The splitting of the reflection peaks at higher angles in cavities C115 and C125 (Fig. 2c and Fig. S9, ESI†) was derived from different dispersions in the transverse magnetic modes and transverse electric modes. Under optical excitation at 405 nm, LP emission was observed from all cavities (Fig. 2d and Fig. S6b, S7b and S9b, ESI†). This emission can be explained on the basis of radiative pumping from the excimer state which is discussed in detail below.

Time-resolved PL spectra

The encapsulated cavity samples (C90, C100, C110, C120) showed LP and excimer emission coupled to external fields[45–47] with a time-dependent relative intensity change (Fig. 3a and Fig. S11a, S12a, S13a, ESI†). We speculated that the distribution of exciton reservoir in such $\lambda/2$ cavities would localise at the centre of the active layer, *i.e.*, at the node of the electric field, soon after the UP excitation. The successive exciton diffusion/energy transfer/light scattering processes may lead to the time dependence of the emission coupled to the external field. While the LP decay profiles differ among cavities (Fig. S14, ESI†), the LP decays mostly followed the profiles of the bare film (excimer emission, Fig. 3c) regardless of the cavity detuning under the same wavelength integration range (shown in grey in Fig. 3a and b). This means the LP decay reflects the density of states (DOS) of the excimer state. The cavity seems to act as a filter cutting out light emission around the resonance region. In contrast, the excimer emission far from the LP state decayed more slowly in the first hundred nanoseconds (Fig. 3c and Fig. 11c, 12c, 13c, ESI†). This is possibly due to the suppression of the emission process in the off-resonant region.[36] The PL decay did not change for samples without a top mirror or films on glass (Fig. S15b–d, ESI†), clarifying that this suppression stems from the cavity structure.

It is worth noting that the delayed emission over hundreds of nanoseconds, which is considered to be derived from triplet–triplet annihilation (TTA), did not change under strong coupling (Fig. 3d). Since the triplet energy of BPEA is estimated to be half of the singlet energy ($E(S_1) = 2.4$ eV, $E(T_1) \sim 1.2$ eV), BPEA can undergo both singlet fission (SF) and TTA.[48,49] Different from the previous report on manipulation of long-lived triplet-derived emission in microcavities,[24] the delayed

profiles overlapped each other regardless of the mirrors. The rapid excimer formation would hinder the effect of strong coupling on spin evolution processes of triplet-pair intermediates which typically proceeds over nanoseconds timescale.[50,51] Therefore, properly controlling intermolecular interactions is necessary to exploit the enhancement under strong coupling.

To compare the relative PL intensity, the time-integrated PL of the cavities and the bare film were calculated (Table 1). We normalized the decays at 525 ns since the delayed components are almost the same among samples. This allowed us to compare the relative intensity of the initial PL to that of the delayed PL, assuming that the delayed PL decay profiles are similar/identical, even if the net absorption intensities differ among the samples. The integrated cavity PL intensity appeared to be weaker than the bare film. As the LP peak approaches the energy of the excimer emission peak, the integrated PL increased. This is a typical feature of LP states populated by radiative pumping which depends on the photonic Hopfield coefficient $|\alpha_\gamma|^2$ (Fig. S6e, S7e, S8e, S9e, ESI†) and the spectral overlap between the LP mode and the excimer emission.[30–33] Since both factors increase as the cavity is detuned negatively from C90 to C120, detected LP emission intensity became stronger (Table 1). The polariton populations for the cavities were distributed toward the bottom of the LPB (Fig. S16, ESI†), which indicates efficient scattering into the energy minimum during the pumping process.

Transient absorption spectrum of the bare ^{tBu}BPEA film

The possible processes involved in the initial decay dynamics, such as singlet fission and excimer formation, were also studied using transient absorption spectroscopy (Fig. S17, ESI†). Following optical excitation at 400 nm, a broad component on the order of 500 nm was observed, which is similar to BPEA dimers.[41] A slight change of the spectra between 500 nm and 600 nm during the first several picoseconds would arise from the relaxation process of excimer. We could not obtain a rise of the triplet as reported for BPEA crystals with $C2/c$ and $Pbcn$ polymorphs, indicating negligible contribution of singlet fission.[48] The decay process of the excimer component with hundreds of picosecond timescale is assigned to singlet–singlet annihilation (SSA). Fast formation of excimer prevents ^{tBu}BEPA from undergoing singlet fission. The charge transfer state of BPEA has been estimated to be 3.30 eV in toluene,[41] which is

Table 1 LP emission peaks and relative values of integrated PL intensity to the one for the bare film (B100) cavity. Decay profiles in Fig. 3d were used. The integrated value ratios to the total one in B100 was also shown in parentheses

Samples	LP emission peak [eV]	Relative values of integrated PL from 0 ns to 125 ns	Relative values of integrated PL from 125 ns to 8.5 μs
B100	—	1.0 (92.5%)	1.0 (7.5%)
C90	2.45	0.063	1.0
C100	2.44	0.071	0.99
C110	2.35	0.18	1.0
C120	2.26	0.22	0.99

14750 | *Phys. Chem. Chem. Phys.*, 2024, **26**, 14745–14753
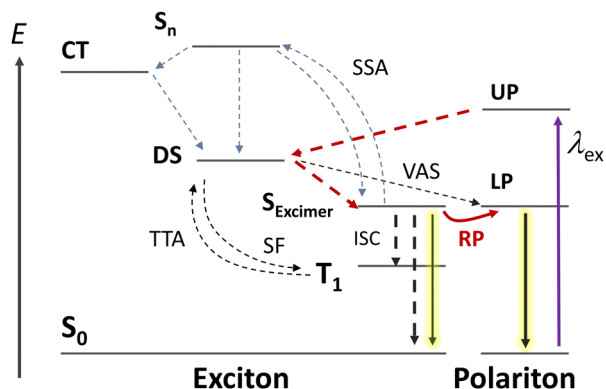
This journal is © the Owner Societies 2024

Fig. 4 Possible intracavity decay dynamics of the ^{tBu}BPEA exciton–polariton materials. Radiative pumping is here abbreviated as RP.

unlikely to be populated from the excimer state ($E_{\text{excimer}} \sim$ 2.2 eV).

Possible excited-state dynamics of polaritons

The excited-state dynamics of the cavity samples is mostly dominated by that of the ^{tBu}BPEA layer (Fig. 4). After optical excitation, a large part of the excitation ends up in the excitonic/dark/reservoir state and relaxes to excimers. The contribution of VAS to the total population dynamics would be small based on the previous simulations suggesting that the VAS mechanism as classically formulated only has a major impact in systems with minimal Stokes shift.[52] Non-radiative processes from the excimer state, such as intersystem crossing (ISC) and internal conversion (IC) are less likely to be modified, given that the change in the potential energy surface of the excimer state is negligible because the excimer state is not itself involved in the strong light-matter coupling. The contribution of SSA, which depends on the density of excimer and its diffusion, seems to be less significant on the ns to ms timescale under the TRPL condition since B100 has about 4 times more absorption than C120 while the PL dynamics are similar (Fig. S15d, ESI†). Therefore, the radiative rate of the excimer plays a major role on LP emission in the first hundreds of nanoseconds. The broad DOS of the excimer state results in the limited amount of LP emission. The state in off-resonance decays non-radiatively or by modes coupled to external fields. Part of the excimers would undergo ISC and TTA and quickly form the excimers again without any change in the delayed component.

Conclusions

In this work, we have investigated the PL dynamics of the strongly coupled microcavities filled with a neat film showing only excimer emission and DOS change in the excited state. A non-symmetric substitution with a *tert*-butyl group at the 2nd position of BPEA resulted in the formation of a dense amorphous neat film after spin coating, which realized a large Rabi splitting over 0.5 eV. Apart from the LP emission, we observed an excimer emission in the off-resonance region, which decayed slower than in the neat film. This suppression of the

radiative process might be useful in photovoltaics to improve energy/electron transfer inside the cavity by avoiding emission losses.[53] Importantly, the DOS of the excimer emission and the radiative pumping process mostly determine the LP emission dynamics. The negligible change in the delayed emission dynamics is probably due to the rapid formation of excimer, which outcompetes the triplet pair-involved processes. Control of the DOS by the proper intramolecular interaction is necessary for manipulating of both short-lived and long-lived species under strong coupling. Further chemical structure-dependent studies would clarify at what point cavities act more than optical filters, leading to the rational design of future room-temperature polariton technologies such as polariton lasers, polariton transistors, and light-emitting diodes.

Author contributions

Conflicts of interest

There are no conflicts to declare.

Acknowledgements

Notes and references

1 J. Kasprzak, M. Richard, S. Kundermann, A. Baas, P. Jeambrun, J. M. J. Keeling, F. M. Marchetti, M. H. Szymańska, R. André, J. L. Staehli, V. Savona, P. B. Littlewood, B. Deveaud and L. S. Dang, Bose–Einstein condensation of exciton polaritons, *Nature*, 2006, **443**, 409–414.

2 K. G. Lagoudakis, M. Wouters, M. Richard, A. Baas, I. Carusotto, R. André, L. S. Dang and B. Deveaud-Plédran, Quantized vortices in an exciton–polariton condensate, *Nat. Phys.*, 2008, **4**, 706–710.

3 A. Amo, J. Lefrère, S. Pigeon, C. Adrados, C. Ciuti, I. Carusotto, R. Houdré, E. Giacobino and A. Bramati, Superfluidity of polaritons in semiconductor microcavities, *Nat. Phys.*, 2009, **5**, 805–810.

4 D. G. Lidzey, D. D. C. Bradley, M. S. Skolnick, T. Virgili, S. Walker and D. M. Whittaker, Strong exciton–photon coupling in an organic semiconductor microcavity, *Nature*, 1998, **395**, 53–55.

5 S. Kéna-Cohen and S. R. Forrest, Room-temperature polariton lasing in an organic single-crystal microcavity, *Nat. Photonics*, 2010, **4**, 371–375.

6 J. D. Plumhof, T. Stöferle, L. Mai, U. Scherf and R. F. Mahrt, Room-temperature Bose-Einstein condensation of cavity exciton-polaritons in a polymer, *Nat. Mater.*, 2014, **13**, 247–252.

7 G. Lerario, A. Fieramosca, F. Barachati and D. Ballarini, Room-temperature superfluidity in a polariton condensate, *Nat. Phys.*, 2017, **13**, 837–841.

8 T. Cookson, K. Georgiou, A. Zasedatelev, R. T. Grant, T. Virgili, M. Cavazzini, F. Galeotti, C. Clark, N. G. Berloff, D. G. Lidzey and P. G. Lagoudakis, A yellow polariton condensate in a dye filled microcavity, *Adv. Opt. Mater.*, 2017, **5**, 1700203.

9 J. A. Hutchison, T. Schwartz, C. Genet, E. Devaux and T. W. Ebbesen, Modifying chemical landscapes by coupling to vacuum fields, *Angew. Chem., Int. Ed.*, 2012, **51**, 1592–1596.

10 J. Mony, C. Climent, A. U. Petersen, K. Moth-Poulsen, J. Feist and K. Börjesson, Photoisomerization efficiency of a solar thermal fuel in the strong coupling regime, *Adv. Funct. Mater.*, 2021, **31**, 2010737.

11 K. Stranius, M. Hertzog and K. Börjesson, Selective manipulation of electronically excited states through strong light–matter interactions, *Nat. Commun.*, 2018, **9**, 1–7.

12 E. Eizner, L. A. Martínez-Martínez, J. Yuen-Zhou and S. Kéna-Cohen, Inverting singlet and triplet excited states using strong light-matter coupling, *Sci. Adv.*, 2019, **5**, eaax4482.

13 Y. Yu, S. Mallick, M. Wang and K. Börjesson, Barrier-free reverse-intersystem crossing in organic molecules by strong light-matter coupling, *Nat. Commun.*, 2021, **12**, 1–8.

14 I. Cho, W. J. Kendrick, A. N. Stuart, P. Ramkissoon, K. P. Ghiggino, W. W. H. Wong and G. Lakhwani, Multi-resonance TADF in optical cavities: suppressing excimer emission through efficient energy transfer to the lower polariton states, *J. Mater. Chem.*, 2023, **11**, 14448–14455.

15 D. M. Coles, N. Somaschi, P. Michetti, C. Clark, P. G. Lagoudakis, P. G. Savvidis and D. G. Lidzey, Polariton-mediated energy transfer between organic dyes in a strongly coupled optical microcavity, *Nat. Mater.*, 2014, **13**, 712–719.

16 X. Zhong, T. Chervy, S. Wang, J. George, A. Thomas, J. A. Hutchison, E. Devaux, C. Genet and T. W. Ebbesen, Non-Radiative Energy Transfer Mediated by Hybrid Light-Matter States, *Angew. Chem., Int. Ed.*, 2016, **55**, 6202–6206.

17 K. Georgiou, R. Jayaprakash, A. Othonos and D. G. Lidzey, Ultralong-Range Polariton-Assisted Energy Transfer in Organic Microcavities, *Angew. Chem., Int. Ed.*, 2021, **60**, 16661–16667.

18 R. Pandya, R. Y. S. Chen, Q. Gu, J. Sung, C. Schnedermann, O. S. Ojambati, R. Chikkaraddy, J. Gorman, G. Jacucci, O. D. Onelli, T. Willhammar, D. N. Johnstone, S. M. Collins, P. A. Midgley, F. Auras, T. Baikie, R. Jayaprakash, F. Mathevet, R. Soucek, M. Du, A. M. Alvertis, A. Ashoka, S. Vignolini, D. G. Lidzey, J. J. Baumberg, R. H. Friend, T. Barisien, L. Legrand, A. W. Chin, J. Yuen-Zhou, S. K. Saikin, P. Kukura, A. J. Musser and A. Rao, Microcavity-like exciton-polaritons can be the primary photoexcitation in bare organic semiconductors, *Nat. Commun.*, 2021, **12**, 1–11.

19 S. Renken, R. Pandya, K. Georgiou, R. Jayaprakash, L. Gai, Z. Shen, D. G. Lidzey, A. Rao and A. J. Musser, Untargeted effects in organic exciton–polariton transient spectroscopy: A cautionary tale, *J. Chem. Phys.*, 2021, **155**, 154701.

20 M. Son, Z. T. Armstrong, R. T. Allen, A. Dhavamani, M. S. Arnold and M. T. Zanni, Energy cascades in donor-acceptor exciton-polaritons observed by ultrafast two-dimensional white-light spectroscopy, *Nat. Commun.*, 2022, **13**, 1–10.

21 L. A. Martínez-Martínez, M. Du, R. F. Ribeiro, S. Kéna-Cohen and J. Yuen-Zhou, Polariton-Assisted Singlet Fission in Acene Aggregates, *J. Phys. Chem. Lett.*, 2018, **9**, 1951–1957.

22 S. Takahashi, K. Watanabe and Y. Matsumoto, Singlet fission of amorphous rubrene modulated by polariton formation, *J. Chem. Phys.*, 2019, **151**, 074703.

23 B. Liu, V. M. Menon and M. Y. Sfeir, The Role of Long-Lived Excitons in the Dynamics of Strongly Coupled Molecular Polaritons, *ACS Photonics*, 2020, **7**, 2292–2301.

24 D. Polak, R. Jayaprakash, T. P. Lyons, L. Á. Martínez-Martínez, A. Leventis, K. J. Fallon, H. Coulthard, D. G. Bossanyi, K. Georgiou, A. J. Petty Ii, J. Anthony, H. Bronstein, J. Yuen-Zhou, A. I. Tartakovskii, J. Clark and A. J. Musser, Manipulating molecules with strong coupling: harvesting triplet excitons in organic exciton microcavities, *Chem. Sci.*, 2020, **11**, 343–354.

25 A. M. Berghuis, A. Halpin, Q. Le-Van, M. Ramezani, S. Wang, S. Murai and J. Gómez Rivas, Enhanced delayed fluorescence in tetracene crystals by strong light-matter coupling, *Adv. Funct. Mater.*, 2019, **29**, 1901317.

26 C. Ye, S. Mallick, M. Hertzog, M. Kowalewski and K. Börjesson, Direct Transition from Triplet Excitons to Hybrid Light-Matter States via Triplet-Triplet Annihilation, *J. Am. Chem. Soc.*, 2021, **143**, 7501–7508.

27 D. M. Coles, P. Michetti, C. Clark, W. C. Tsoi, A. M. Adawi, J-S. Kim and D. G. Lidzey, Vibrationally assisted polariton-relaxation processes in strongly coupled organic-semiconductor microcavities, *Adv. Funct. Mater.*, 2011, **21**, 3691–3696.

28 L. Mazza, S. Kéna-Cohen and P. Michetti, and G. C. La Rocca, Microscopic theory of polariton lasing via vibronically assisted scattering, *Phys. Rev. B: Condens. Matter Mater. Phys.*, 2013, **88**, 075321.

29 A. V. Zasedatelev, A. V. Baranikov, D. Urbonas, F. Scafirimuto, U. Scherf, T. Stöferle, R. F. Mahrt and P. G. Lagoudakis, A room-temperature organic polariton transistor, *Nat. Photonics*, 2019, **13**, 378–383.

30 P. Michetti and G. C. La Rocca, Simulation of J-aggregate microcavity photoluminescence, *Phys. Rev. B: Condens. Matter Mater. Phys.*, 2008, **77**, 195301.

14752 | *Phys. Chem. Chem. Phys.*, 2024, **26**, 14745–14753

This journal is © the Owner Societies 2024

31 P. Michetti and G. C. La Rocca, Exciton-phonon scattering and photoexcitation dynamics in J-aggregate microcavities, *Phys. Rev. B: Condens. Matter Mater. Phys.*, 2009, **79**, 035325.

32 G. H. Lodden and R. J. Holmes, Electrical excitation of microcavity polaritons by radiative pumping from a weakly coupled organic semiconductor, *Phys. Rev. B: Condens. Matter Mater. Phys.*, 2010, **82**, 125317.

33 R. T. Grant, P. Michetti, A. J. Musser, P. Gregoire, T. Virgili, E. Vella, M. Cavazzini, K. Georgiou, F. Galeotti, C. Clark, J. Clark, C. Silva and D. G. Lidzey, Efficient radiative pumping of polaritons in a strongly coupled microcavity by a fluorescent molecular dye, *Adv. Opt. Mater.*, 2016, **4**, 1615–1623.

34 T. Khazanov, S. Gunasekaran, A. George, R. Lomlu, S. Mukherjee and A. J. Musser, Embrace the darkness: An experimental perspective on organic exciton–polaritons, *Chem. Phys. Rev.*, 2023, **4**, 041305.

35 S. A. Furman and A. V. Tikhonravov, *Basics of Optics of Multilayer Systems*, Atlantica Seguier Frontieres, Paris, 1992, vol. 0, p. 1–102.

36 A. Kavokin, J. J. Baumberg, G. Malpuech and F. P. Laussy, *Microcavities*, Oxford University Press, 2007.

37 M. J. Frisch, G. W. Trucks, H. B. Schlegel, G. E. Scuseria, M. A. Robb, J. R. Cheeseman, G. Scalmani, V. Barone, B. Mennucci, G. A. Petersson, H. Nakatsuji, M. Caricato, X. Li, H. P. Hratchian, A. F. Izmaylov, J. Bloino, G. Zheng, J. L. Sonnenberg, M. Hada, M. Ehara, K. Toyota, R. Fukuda, J. Hasegawa, M. Ishida, T. Nakajima, Y. Honda, O. Kitao, H. Nakai, T. Vreven, J. A. Montgomery, Jr., J. E. Peralta, F. Ogliaro, M. Bearpark, J. J. Heyd, E. Brothers, K. N. Kudin, V. N. Staroverov, T. Keith, R. Kobayashi, J. Normand, K. Raghavachari, A. Rendell, J. C. Burant, S. S. Iyengar, J. Tomasi, M. Cossi, N. Rega, J. M. Millam, M. Klene, J. E. Knox, J. B. Cross, V. Bakken, C. Adamo, J. Jaramillo, R. Gomperts, R. E. Stratmann, O. Yazyev, A. J. Austin, R. Cammi, C. Pomelli, J. W. Ochterski, R. L. Martin, K. Morokuma, V. G. Zakrzewski, G. A. Voth, P. Salvador, J. J. Dannenberg, S. Dapprich, A. D. Daniels, O. Farkas, J. B. Foresman, J. V. Ortiz, J. Cioslowski and D. J. Fox, *Gaussian 09, Revision D.01*, Wallingford CT, 2013.

38 D. G. Bossanyi, M. Matthiesen, S. Wang, J. A. Smith, R. C. Kilbride, J. D. Shipp, D. Chekulaev, E. Holland, J. E. Anthony, J. Zaumseil, A. J. Musser and J. Clark, Emissive spin-0 triplet-pairs are a direct product of triplet-triplet annihilation in pentacene single crystals and anthradithiophene films, *Nat. Chem.*, 2021, **13**, 163–171.

39 T. Serevičius, R. Komskis, P. Adomėnas, O. Adomėnienė, V. Jankauskas, A. Gruodis, K. Kazlauskas and S. Juršėnas, Non-symmetric 9,10-diphenylanthracene-based deep-blue emitters with enhanced charge transport properties, *Phys. Chem. Chem. Phys.*, 2014, **16**, 7089–7101.

40 N. J. Hestand and F. C. Spano, Molecular Aggregate Photophysics beyond the Kasha Model: Novel Design Principles for Organic Materials, *Acc. Chem. Res.*, 2017, **50**, 341–350.

41 Y. J. Bae, D. Shimizu, J. D. Schultz, G. Kang, J. Zhou, G. C. Schatz, A. Osuka and M. R. Wasielewski, Balancing Charge Transfer and Frenkel Exciton Coupling Leads to Excimer Formation in Molecular Dimers: Implications for Singlet Fission, *J. Phys. Chem. A*, 2020, **124**, 8478–8487.

42 M. S. Myong, R. M. Young and M. R. Wasielewski, Excimer Diffusivity in 9,10-Bis(phenylethynyl)anthracene Assemblies on Anodic Aluminum Oxide Membranes, *J. Phys. Chem. C*, 2021, **125**, 24498–24504.

43 D. G. Lidzey, D. D. Bradley, A. Armitage, S. Walker and M. S. Skolnick, Photon-mediated hybridization of frenkel excitons in organic semiconductor microcavities, *Science*, 2000, **288**, 1620–1623.

44 V. Savona, L. C. Andreani, P. Schwendimann and A. Quattropani, Quantum well excitons in semiconductor microcavities: Unified treatment of weak and strong coupling regimes, *Solid State Commun.*, 1995, **93**, 733–739.

45 A. K. Ghatak, Leaky modes in optical waveguides, *Opt. Quantum Electron.*, 1985, **17**, 311–321.

46 F. Herrera and F. C. Spano, Absorption and photoluminescence in organic cavity QED, *Phys. Rev. A*, 2017, **95**, 053867.

47 L. Huang, L. Xu, D. A. Powell, W. J. Padilla and A. E. Miroshnichenko, Resonant leaky modes in all-dielectric metasystems: Fundamentals and applications, *Phys. Rep.*, 2023, **1008**, 1–66.

48 Y. J. Bae, G. Kang, C. D. Malliakas, J. N. Nelson, J. Zhou, R. M. Young, Y.-L. Wu, R. P. Van Duyne, G. C. Schatz and M. R. Wasielewski, Singlet Fission in 9,10-Bis(phenylethynyl)anthracene Thin Films, *J. Am. Chem. Soc.*, 2018, **140**, 15140–15144.

49 V. Gray, A. Dreos, P. Erhart, B. Albinsson, K. Moth-Poulsen and M. Abrahamsson, Loss channels in triplet-triplet annihilation photon upconversion: importance of annihilator singlet and triplet surface shapes, *Phys. Chem. Chem. Phys.*, 2017, **19**, 10931–10939.

50 E. A. Wolf, D. M. Finton, V. Zoutenbier and I. Biaggio, Quantum beats of a multiexciton state in rubrene single crystals, *Appl. Phys. Lett.*, 2018, **112**, 083301.

51 T. S. C. MacDonald, M. J. Y. Tayebjee, M. I. Collins, E. Kumarasamy, S. N. Sanders, M. Y. Sfeir, L. M. Campos and D. R. McCamey, Anisotropic Multiexciton Quintet and Triplet Dynamics in Singlet Fission via Pulsed Electron Spin Resonance, *J. Am. Chem. Soc.*, 2023, **145**, 15275–15283.

52 E. Hulkko, S. Pikker, V. Tiainen, R. H. Tichauer, G. Groenhof and J. J. Toppari, Effect of molecular Stokes shift on polariton dynamics, *J. Chem. Phys.*, 2021, **154**, 154303.

53 L. C. Hirst and N. J. Ekins-Daukes, Fundamental losses in solar cells, *Prog. Photovoltaics Res. Appl.*, 2011, **19**, 286–293.

This journal is © the Owner Societies 2024

Phys. Chem. Chem. Phys., 2024, **26**, 14745–14753 | **14753**